Intraoral low-temperature degradation of monolithic zirconia dental prostheses: 5-year results of a prospective clinical study with *ex vivo* monitoring

V. Koenig[a,b], T. Douillard[c], J. Chevalier[c], F. Amiard[d], M. Lamy de la Chapelle[d], S. Le Goff[e], A. Vanheusden[a,b], N. Dardenne[f], C. Wulfman[a,e*] & A. Mainjot[a,b*,**]

* These authors contributed equally.

[a] Dental Biomaterials Research Unit (d-BRU), University of Liège (ULiège), 45 Quai G. Kurth, Liège, 4020, Belgium.
[b] Department of Fixed Prosthodontics, Institute of Dentistry, University of Liège Hospital (CHU), 45 Quai G. Kurth, Liège, 4020, Belgium.
[c] Université de Lyon, INSA Lyon, CNRS, MATEIS, UMR 5510, F-69621 Villeurbanne, France.
[d] Institut des Molécules et Matériaux du Mans (IMMM - UMR6283), Université du Mans, avenue Olivier Messiaen, 72085 Le Mans Cedex 9.
[e] Unité de Recherches en Biomatériaux Innovants et Interfaces (URB2i) – EA4462, Faculté de Chirurgie Dentaire, Université Paris Descartes, Sorbonne Paris-Cité, Montrouge, 92120, France.
[f] Department of Public Health, University of Liège, 4000 Liège, Belgium.

**Corresponding author: Amélie Mainjot. Dental Biomaterials Research Unit (d-BRU) and Department of Fixed Prosthodontics, Institute of Dentistry, University of Liège (ULiège) and University of Liège Hospital (CHU), 45 Quai G. Kurth, Liège, 4020, Belgium. E-mail address: a.mainjot@chuliege.be

Abstract

Objectives: To investigate the 5-year intraoral evolution and kinetics of low-temperature degradation (LTD) of second-generation monolithic prostheses made of 3% molar yttrium-doped tetragonal zirconia polycrystal (3Y-TZP) and the influence of masticatory mechanical stresses and glaze layer on this evolution.

Methods: A total of 101 posterior tooth elements were included in this prospective clinical study, which comprised *ex vivo* LTD monitoring (at baseline, 6 months, 1 year, 2 years, 3 years, and 5 years) using Raman spectroscopy (n=2640 monoclinic phase measurement points per evaluation time) and scanning electron microscopy (SEM). Four types of areas (1–2 mm^2 surface, six on molars, and four on premolars) were analysed on each element surface: occlusal, axial, glazed, or unglazed. Raman mapping, high-resolution SEM, and focused ion beam-SEM were performed on selected samples.

Results: The dental prostheses developed a tetragonal-to-monoclinic transformation at the extreme surface of the material after six months in a buccal environment, and this process increased

significantly over time. Over the five years of monitoring, the transformation developed nonuniformly with the presence of localised clusters of monoclinic grains. Tribological stresses generate grain pull-out from these clusters, which may raise questions regarding the release of 3Y-TZP nanoparticles into the body. The prosthesis fracture rate was 4.5% after 5 years.

Significance: LTD developed *in vivo* on the surfaces of 3Y-TZP dental prostheses and progressed slowly but significantly over time, up to 5 years investigation. However, the effects of aging on the failure rate recorded and of zirconia nanoparticles released into the body require further investigation.

Keywords: 3Y-TZP, computer-aided design/computer-aided manufacturing, Raman spectroscopy, biomaterials, aging, *t-m* transformation

1. Introduction

In the early 2000s, low-temperature degradation (LTD) of 3% molar yttrium-doped tetragonal zirconia polycrystal (3Y-TZP) ceramics induced significant clinical consequences in orthopaedic devices, such as the fracture of approximately 600–800 zirconia heads within two years of implantation [1]. Seven batches of the Prozyr® material, manufactured using tunnel furnaces suspected to increase LTD susceptibility, were affected [2]. Numerous lab-scale studies on the effects of LTD on implants have been conducted [3-9], while several assessments related to *in vivo* aging have been performed through retrospective explant analyses. These results confirmed many of the features discussed at the lab scale and highlighted the surface degradation of retrieved zirconia hip implants [2, 10-14] and/or related strong osteolysis [15-17]. The results showed that LTD was responsible for some clinical failures resulting from the use of zirconia in orthopaedics. The Prozyr® heads broke because of crack propagation which initiated in the micro-cracked, transformed region, which was loaded in tension. Many retrieved heads exhibited extensive grain pull-out, which resulted in material debris around the implant, chronic inflammation, and, in the worst cases, osteolysis. These issues, in particular the "Prozyr® failures," had a negative impact on the use of Y-TZP in the field of orthopaedics, despite contrasting results from zirconia heads of different compositions, which exhibited strong performances and low wear rates [18, 19].

In contrast to its abandonment in orthopaedics in favor of zirconia-toughened alumina composites, the use of Y-TZP as implants, abutments, and crowns has increased in the dental field in the last decade owing to its better aesthetic properties when compared with metal alloys and its higher mechanical resistance than glass-ceramics, owing to its unique phase transformation toughening at room temperature. In particular, the important economic development of digital technologies in the dental field has resulted in the progressive disappearance of the handcrafted veneering process of prostheses and the large production of full zirconia prostheses produced by computer-aided design/computer-aided manufacturing (CAD/CAM) processes. However, recently developed dental zirconia materials have been shown to exhibit important metastable behaviour *in vitro*, which could promote LTD [20, 21], while a systematic review concluded that LTD could significantly decrease the flexural strength of 3Y-TZP dental ceramics, particularly in samples where 50% of the surface is transformed [22-24]. Moreover, ISO 13356-2015 [25] states that the monoclinic phase content should not exceed 25% in Y-TZP implants after autoclave aging for biomedical purposes. Nevertheless, *in vitro* autoclave aging conditions are far from the body environment in terms of pressure and temperature, and they do not consider exposure to salivary ionic solution, acidic beverages, constant changes in pH, and especially the effects of masticatory tribological stress on material aging.

Mechanical stress was shown to accelerate Y-TZP degradation in hip prostheses [5, 14, 26]. However, to date, LTD in dental prostheses under real conditions for use *in vivo* has not been investigated.

Therefore, an original clinical research protocol, including *ex vivo* analyses, was designed to investigate the intraoral development and kinetics of LTD in second-generation zirconia dental prostheses over five years, as well as the influence of masticatory mechanical stress and glaze on this process [27]. The results of the 2-year follow-up in this prospective clinical study have been described previously [28, 29]. This paper reports the results of this project.

2. Materials and methods

2.1. Study design

The protocol for this prospective clinical study was approved by the Ethics Committee of the University Hospital Center (CHU) of Liege and was registered in the ClinicalTrials.gov database (Identifier: NCT02150226). The authors complied with the Strobe guidelines. The study design is illustrated in Figure 1. Written informed consent was obtained from all the patients before inclusion. The patients were treated by four experienced operators at the Department of Fixed Prosthodontics, Institute of Dentistry, CHU of Liege, Belgium. The eligibility criteria included the need for a molar or premolar crown (maximum of six tooth elements per patient). Restorations were realised either on natural teeth or dental implants, and bridges were also included, provided they were on implants and limited to three elements. Patients without teeth or removable prostheses opposite the prostheses were excluded. Forty-seven patients with 101 tooth elements were included in the study. The sample descriptions are presented in Table 1.

2.2. Clinical procedure and prostheses manufacturing

Clinical procedures related to tooth preparation and impression were performed according to standardised criteria and manufacturer's recommendations. The detailed clinical protocol has been presented in previous publications [27, 28].

Zirconia restorations (Lava Plus, 3M ESPE, Seefeld, Germany) were designed to allow Raman analysis, as illustrated in Figures 2 and 3. The contact point areas with opposite teeth were shaped to obtain a flat surface of 1-2 mm^2. If needed, contact points with the opposite teeth were adjusted in the mouth, following the manufacturer's recommendations.

Two types of areas were analysed: areas subjected to masticatory mechanical stress (MS+, i.e., contact point areas with the opposite teeth) or not (MS-, i.e., axial surfaces of the crowns on their lingual or buccal side). Half of the analysed areas were glazed (G+) and half were left unglazed (G-). In the MS- areas, the buccal surface was systematically glazed, while the lingual surface was left unglazed. Half of the MS+ areas were randomly selected to remain unglazed. The glaze (IPS Empress stains and eMax Ceram glaze, Ivoclar Vivadent, Schaan, Liechtenstein) was sintered at 780°C for 1 min.

Baseline analyses were performed prior to placement. After 6 months, the restorations were removed for *ex vivo* analyses, and provisional restorations replaced the zirconia restorations. Evaluations were repeated after one-year, two-year, three-year, and five-year intraoral stay. The four-year follow-up could not be performed because of the Covid-19 pandemic. All areas were encircled with permanent ink before *ex vivo* analyses and registered with a picture.

2.3. *Ex vivo* analyses

Ex vivo analyses included (1) phase transformation using Raman spectroscopy and (2) glaze wear using conventional scanning electron microscopy (SEM). Sample descriptions of the *ex vivo* analysed areas (n=528) and measurement points (MPs) (n=2640) are presented in Table 1. Moreover, additional Raman mapping, high-resolution SEM, and focused ion beam (FIB)-SEM were performed on selected samples to verify the hypotheses formulated after the Raman spectroscopy analysis and conventional SEM results.

2.3.1. Raman Spectroscopy

Five MPs were randomly chosen for each MS+ and MS- area (30 measurements for a molar and 20 measurements for a premolar). Consequently, analyses were performed on 2640 MPs at each evaluation time. The Raman spectra were recorded using a Raman microspectrometer (LabRAM, Horiba Scientific). The excitation laser was a HeNe laser (632 nm) with 1 mW power focused at the surface, and the Raman spectra were acquired using a charge-coupled device detector (Horiba-Jobin Yvon) with a spectral resolution of 1 cm^{-1}. A confocal pinhole with adjustable diameter was used for confocal detection, and an 80× objective (numerical aperture 0.75) was used to achieve a 1 μm^3 resolution (lateral × axial). A pinhole aperture of 1.99 µm was used to reach a collection depth of 1.44 µm. The depth was determined using the calibration wedge method [30].

The collected spectra were analysed, and the transformed monoclinic volume fraction (V_{fm}), which is a measure of the transformation volume ratio in the confocally probed volume, was estimated using Eq. (1), initially proposed by Clarke and Adar [31]:

$$V_{fm} = \frac{I_m^{178} + I_m^{189}}{0.33(I_t^{145} + I_t^{256}) + I_m^{178} + I_m^{189}}$$

where I_m and I_t are the peak intensities (superscript wavenumbers) of the monoclinic and tetragonal phases, respectively. Raman peak positions and intensities were obtained by fitting the Raman spectra with Lorentzian curves using Origin 8 software (OriginLab, Northampton, MA, USA).

2.3.2. SEM observations

After the Raman spectroscopy experiments, the restorations were gold-coated and observed using a JSM-6400 conventional SEM (JEOL Ltd., Tokyo, Japan) to determine the glaze wear.

2.3.3. Additional experimentations on selected samples

2.3.3.1. Raman mapping

Raman spectroscopy mapping was performed on one crown immediately after machining (control), two crowns after the 3-year follow-up, and one crown and two bridges after the 5-year follow-up. Raman mapping was performed using a Raman microspectrometer (Alpha300 Apyron, WITEC). The material was excited with a HeNe laser (633 nm), and Raman spectra were recorded in a backscattering configuration using a 20X objective (numerical aperture = 0.50) with a spectral resolution of 1.77 cm^{-1}.

For the surface characterisation, the mapping of a surface area of 100×100 μm^2 with a step size of 3.33 µm was first conducted. When the *m* phase was detected, high-resolution mapping of an area of 25×25 μm^2 with a step size of 700 nm was performed. The depth profiles of the selected zones were conducted along one line at different depths with a step size of 1 µm.

For each map, the recorded signal was integrated with the spectral range of 24 cm^{-1} centred at 184 cm^{-1} using the built-in Raman spectrometer software. The signal value was automatically transformed to a colour scale using software.

2.3.3.2. High-resolution SEM observations without gold coating

High-performance SEM (Supra 55VP; Carl Zeiss Microscopy GmbH, Oberkochen, Germany) was performed on one crown immediately after machining (control), one crown after the 2-year follow-

up, and one crown and one bridge after the 5-year follow-up. The microscope was fitted with a variable-pressure secondary electron (VPSE) detector. This VPSE detector comprises a specific arrangement of detectors designed to obtain electron-similar imaging in a gaseous environment (up to 133 Pa of gaseous nitrogen), allowing the observation of non-conductive samples without the usual requirement of a metalised surface coating. Thus, high-resolution topographic SEM imaging was performed on the MS+ and MS- areas with an accelerating voltage of 10 kV and a pressure of 10 Pa without any coating.

2.3.3.3. FIB-SEM

Further evaluations of the two crown subsurfaces before and 5 years after intraoral aging were completed using FIB cross-sections. These analyses were performed using a FIB/SEM workstation (NVision 40; Carl Zeiss Microscopy GmbH, Oberkochen, Germany). To minimise the curtain effect introduced by gallium ion beam milling (i.e., vertical stripes on the cross-section induced by ion milling) and to protect the sample surface from implantation, in-situ ion beam-induced carbon deposition was performed over the areas of interest. Subsequently, trenches were milled to a depth that freed up a cross-sectional surface allowing assessing the LTD depth (width of 20µm and depth between 15 and 20µm). Settings for a 30 kV ion accelerating voltage with decreasing beam currents (27nA, 13nA, 1.5nA, and 700 pA) were used to reach a suitable cross-section for SEM imaging and to avoid any ion beam-induced monoclinic transformation. SEM imaging was performed at 1.5 KeV simultaneously with secondary electrons (SE) and energy-filtered backscattered electrons (BSE). BSE signals lead to strong crystallographic contrast imaging which is useful for identifying signs of twinning associated with the tetragonal-monoclinic transformation. The SEM imaging allowed us to better check for cracks.

2.4. Statistical analysis

2.4.1. Sample size

The statistical unit was the tooth element characterised by its maximum LTD value measured at each time point.

LTD is expected to induce a significant decrease in material flexural strength when 50% of the sample surface undergoes a tetragonal-to-monoclinic (*t-m*) transformation [24]. The overall proportion (π) of such treatment failures was defined as the primary outcome measure of the study. The study rationale was to reject the proposed treatment for $\pi > 0.20$: more than 20% of the treatment failures over time. Assuming a significance level (α) of 1% (Bonferroni correction for multiple time testing), a power 1-β of 90%, a proportion π of at most 0.08 (margin 0.12), and a one-sided Z test for

a binomial proportion of 0.20, a sample size (N) of 91 teeth was needed to detect > 20% of treatment failures at each data point collection. The sample size was increased to a minimum of 100 teeth to account for correlations between the teeth within the subjects and study withdrawal.

2.4.2. Statistical methods

The collected data were expressed as mean ± standard deviation for quantitative variables and a frequency table for categorical variables. The time evolution of the transformation was analysed using a generalised mixed binomial model (GLMM). The time, group, and interaction effects were also tested. Contrast analyses were performed to test for the differences between each time point. Owing to the presence of excessive zeros, the transformation percentage over time was analysed using a zero-inflated non-negative binomial regression for repeated measurements globally and according to area. The effect of glaze and grinding procedures for contact point adjustments on the transformation with time was also analysed using a GLMM, globally, and according to the type of area (MS+ or MS-).

Results were considered statistically significant when p-value was ≤ 0.05. Data analysis was performed using GraphPad Prism (GraphPad Software, San Diego, CA, USA), the SAS (version 9.4) statistical package, and R version 3.6.1.

3. Results

3.1. Raman spectroscopy

The presence of the monoclinic phase significantly increased between baseline and 5 years, as demonstrated by the evolution of the percentage of MPs+ in the MS- and MS+ areas (Table 3, Figure 4a). At baseline and 6 months, all transformation-positive areas presented only one MP+ out of five MPs (Table 2), which explains the low mean V_{fm} values presented in Table 3. The increase in V_{fm} values was also statistically significant between baseline and 5 years (Table 3). However, a significant decrease in the global MP+ percentage was observed between years 2 and 3.

The results showed significant differences between the MS+ and MS- areas in terms of the evolution of MP+ presence, with a higher increase in MS- areas ($p<0.0001$). The *t-m* transformation was detected at baseline, mostly in MS+, and was significantly associated ($p=0.0003$) with prosthesis grinding using a diamond bur to adjust the contact points with the opposite teeth (34% of MS+ areas had to be adjusted). In MS+ areas, the percentage of MP+50% was significantly decreased between

baseline and 5 years (Table 3, Figure 4b). No significant differences were observed between G+ and G- areas.

3.2. SEM observations

The SEM results revealed that the glaze was worn out in most of the MS+ areas (70.2% of cusps) after 6 months and in all of them after 1, 2, 3, and 5 years (Figures 5a, 5b, and 5c). However, this did not occur in the MS- areas (Figure 5d).

3.3. Raman mapping

Images arising from Raman wide mapping are presented in Figure 6. The yellow and red images (Figures 6d, 6g, 6j, and 6m) were combined to provide the spectral maps (Figures 6c, 6e, 6h, 6q, and 6n). The peaks at approximately 180 cm^{-1} in the yellow spectrum were assigned to the monoclinic phase (Figures 6e, 6h, 6k, and 6n). The analyses revealed the presence of localized clusters of transformed grains (yellow spots) in both the MS- and MS+ areas of the prostheses after 3 years and 5 years of aging, respectively. More clusters were observed in the MS- area than in the MS+ area (Figures 6f, 6i, 6l, and 6o). No transformation was detected in the control sample (Figure 6a). Depth mapping revealed that the transformation seems to extend from the surface towards the interior up to several microns.

3.4. High-resolution SEM observations without gold coating

After 2 and 5 years, high-resolution SEM images illustrate the effect of tribological damage on the MS+ areas (Figures 7d and 7f). The surface appeared polished with generalised grain pull-out, especially in the MS+ areas.

In the MS- areas, there was less grain pull-out and no crushing (Figure 7c). After 5 years, crushed grains were also observed in the MS- areas (Figure 7e). No grain pull-out was observed in the control sample (Figures 7a and 7b), and native grains and grain boundaries were clearly observed at the surface.

3.5. FIB-SEM observations

At 5 years, the FIB-SEM observations of sample surface revealed typical ‘faceting’ of some zirconia grains on an approximately 1-micron depth layer from the surface (Figure 8c and 8d). The faceted

grains are monoclinic, and the contrast observed is typical of twinning occurring during the *t-m* transition [32]. Subsurface microcracks were also observed in this layer (Figure 8e). *T-m* transformation was not observed in the control crown (Figures 8a and 8b).

3.6. Fractures

Two prostheses were lost because of material fracture after 2 and 5 years. Moreover, only one prosthesis had a minor fracture. The prosthesis fracture rate was 4.5% after five years. Overall survival rate at 5 years was 88.1% (six prostheses were lost due to tooth fracture, periodontal disease, or implant loss).

4. Discussion

The 2-year results of this study [28] showed that LTD develops in 3Y-TZP monolithic restorations 6 months after intraoral placement and progresses nonuniformly over time, with the presence of localised clusters of transformed grains. The results at five years show the slow continuity of this process, which remains non-uniform and limited to the extreme surface of the material. The increase in V_{fm} values was statistically significant between baseline and 5 years but remained very low, with the overall image of a few monoclinic spots distributed over the surface (the percentage of transformed regions was still quite low). Raman mapping revealed the presence of localised clusters of transformed grains in both the MS- and MS+ areas of the crowns after 3 and 5 years of aging. These clusters may result from the autocatalytic nature of the phase-transformation nucleation and growth processes [1]. These results confirm the *in vitro* observations of Zhang *et al.* using XRD and Raman spectroscopy [33]. Depth mapping revealed that the transformation propagated inwards from the surface by several microns. However, the FIB-SEM images showed a thinner, constant layer of 1-2 transformed grains on the extreme surface of the sample. Because the FIB-SEM technique allows direct observation of the samples, the observed differences in depth measurements by Raman mapping may be due to certain artefacts. Indeed, if the material is scattered in nature, the confocality can change along the z-axis, inducing an aberration of a few microns [34]. Finally, it must be noted that the *m* phase detected at baseline was significantly correlated with prosthesis grinding using a diamond bur to adjust the contact points with the opposite teeth, generating a stress-induced transformation [20].

In the occlusal areas, tribological stresses led to crushing of the surface and pull-out of the grains from the clusters, as described in the 2-year follow-up, which explains the different evolution of the

transformation in the MS+ and MS- areas. In the MS+ areas, high-resolution SEM images clearly show this grain pull-out and polishing of the surface, which appears plastically deformed, as previously observed in hip prostheses [4, 6, 35, 36]. It is likely that LTD initially induces surface roughness and localised microcracking and that tribological stresses cause monoclinic grains to pull away as the transformation progresses (Figure 9). Indeed, in the MS- areas, Raman mapping showed more clusters of transformed grains, and the surface exhibited less grain pull-out and no crushing compared with the MS+ areas. However, grain pull-out in the MS- areas was greater after 5 years than after 2 years, perhaps because of different friction phenomena, such as the effect of toothbrushing. The pull-out of monoclinic grains led to an underestimation of the LTD process when studied using *m*-phase quantification. This also raises questions regarding the release of 3Y-TZP nanoparticles (grains measuring approximately 0.3 microns in diameter) into the body. Toxicological studies on zirconium oxide (ZrO_2) nanoparticles are limited and the results are controversial. Some studies have reported that ZrO_2 nanoparticles can induce mild [37, 38] or no cytotoxic effects [39-41]. Other authors have pointed out that ZrO_2 nanoparticles have better biocompatibility than other nanomaterials such as ferric oxide, titanium dioxide, and zinc oxide [38, 42-44]. However, ZrO_2 nanoparticles can induce toxic effects at high concentrations, affecting cell viability, inducing apoptosis and necrosis, and changing cell morphology [45]. Fortunately, zirconia debris is swallowed and does not cause local chronic inflammation of the surrounding tissues or osteolysis, as is the case with hip prostheses.

After 5 years, there was still no significant difference between the percentages of MPs+ in the G+ and G- areas, confirming that glaze cannot be considered a protection against LTD. Glaze thickness is very low (0.1 to 0.2 µm) and wears away rapidly in most MS+ areas after 6 months and in all areas after 1 year, due to the presence of tribological stresses [20]. In the MS- areas, glazes did not wear away, and the hypotheses for LTD development in these areas were diffusion of water through the glaze layer during firing [46, 47] or intraoral stay. These results contradict those of two *in vitro* studies [48, 49] in which crowns subjected to mechanical stress showed a significant increase in the monoclinic phase in areas of glaze wear, in contrast to specimens with intact glazes, which showed a stable level of the *m*-phase. However, in these studies, contact with water reduced over time and did not favour diffusion.

Regarding the impact of LTD on prosthesis survival, the fracture rate was 2.6% at 2 years (n=2) and 4.5% (n=3) at 5 years, which is slightly lower than the 5-year fracture rate of monolithic glass-ceramic bonded partial restorations (5.9%), while 3Y-TZP is a supposed to be significantly more resistant [50]. Similarly, a recent meta-analysis of the clinical performance of dental implant-supported crowns

showed that zirconia materials had a slightly lower fracture rate than other ceramic materials [51]. In fact, the impact of LTD development on 3Y-TZP dental zirconia appears to be fairly low in terms of prosthesis life compared to hip prostheses. However, it cannot be ruled out that this process may have contributed to the major and minor fractures observed, as other authors suspect [52]. More recently, novel, highly translucent zirconia varieties that utilise a higher proportion of yttria have been developed; thus, there is an increase in the cubic phase content and a decrease in the tetragonality of the t phase. These restorations exhibit increased LTD resistance because of the higher cubic phase content (yttria-partially stabilised zirconia (Y-PSZ) with 4 or 5 mol%: 4Y-PSZ contains more than 25% of the cubic phase, and 5Y-PSZ contains more than 50%). However, as the cubic phase does not undergo stress-induced transformation, the toughness of these materials is significantly lower than that of 3Y-TZP materials (<700 MPa flexural strength for 5Y-PSZ). Therefore, their indications are limited, particularly for the fabrication of multi-unit restorations [21, 49]. One of the main challenges in developing dental zirconia materials with reduced susceptibility to aging is the trade-off between toughness, LTD resistance, and translucency, which are mandatory properties for dental restorations, unlike hip prostheses.

Finally, it must be stressed that zirconia is not 'a material' but a family of sophisticated materials with varying compositions, microstructures, and manufacturing processes, which can significantly influence their resistance to LTD.

5. Conclusion

LTD develops on the extreme surface of 3Y-TZP monolithic prostheses after 6 months in the buccal environment, and this process increases significantly with time, whereas glazing is not protective. The *t-m* transformation progresses slowly and nonuniformly in the presence of localised clusters of monoclinic grains. In addition, tribological stress causes monoclinic grains to pull out of the clusters, raising questions regarding the release of 3Y-TZP nanoparticles into the body.

Acknowledgments

The authors declare that they have no competing interests related to the authorship and/or publication of this article. The authors thank 3M for providing the restorations used in this study and for the partial funding. The company had no authority over the study design and did not influence the decision to submit the report for publication. We would also like to thank the Consortium Lyon Saint-Etienne de Microscopie (www.clym.fr) for providing access to the FIB/SEM.

References

[1] Chevalier J, Gremillard L, Virkar AV, Clarke DR. The Tetragonal-Monoclinic Transformation in Zirconia: Lessons Learned and Future Trends. Journal of the American Ceramic Society. 2009;92:1901-20.
[2] Chevalier J. What future for zirconia as a biomaterial? Biomaterials. 2006;27:535-43.
[3] Cattani-Lorente M, Scherrer SS, Ammann P, Jobin M, Wiskott HW. Low temperature degradation of a Y-TZP dental ceramic. Acta biomaterialia. 2011;7:858-65.
[4] Chevalier J, Gremillard L, Deville S. Low temperature degradation of zirconia and implications on biomedical implants. Annual Review of Materials Research. 2007;37:1-32.
[5] Douillard T, Chevalier J, Descamps-Mandine A, Warner I, Galais Y, Whitaker P, et al. Comparative ageing behaviour of commercial, unworn and worn 3Y-TZP and zirconia-toughened alumina hip joint heads. J Eur Ceram Soc. 2012;32:1529-40.
[6] Gremillard L, Martin L, Zych L, Crosnier E, Chevalier J, Charbouillot A, et al. Combining ageing and wear to assess the durability of zirconia-based ceramic heads for total hip arthroplasty. Acta biomaterialia. 2013;9:7545-55.
[7] Munoz-Tabares JA, Jimenez-Pique E, Anglada M. Subsurface evaluation of hydrothermal degradation of zirconia. Acta Materialia. 2011;59:473-84.
[8] Samodurova A, Kocjan A, Swain MV, Kosmac T. The combined effect of alumina and silica co-doping on the ageing resistance of 3Y-TZP bioceramics. Acta biomaterialia. 2015;11:477-87.
[9] Gremillard L, Chevalier J, Martin L, Douillard T, Begand S, Hans K, et al. Sub-surface assessment of hydrothermal ageing in zirconia-containing femoral heads for hip joint applications. Acta biomaterialia. 2018;68:286-95.
[10] Catledge SA, Cook M, Vohra YK, Santos EM, McClenny MD, David Moore K. Surface crystalline phases and nanoindentation hardness of explanted zirconia femoral heads. J Mater Sci Mater Med. 2003;14:863-7.
[11] Haraguchi K, Sugano N, Nishii T, Miki H, Oka K, Yoshikawa H. Phase transformation of a zirconia ceramic head after total hip arthroplasty. J Bone Joint Surg Br. 2001;83:996-1000.
[12] Santos EM, Vohra S, Catledge SA, McClenny MD, Lemons J, Moore KD. Examination of surface and material properties of explanted zirconia femoral heads. J Arthroplasty. 2004;19:30-4.
[13] Fernandez-Fairen M, Blanco A, Murcia A, Sevilla P, Gil FJ. Aging of retrieved zirconia femoral heads. Clin Orthop Relat Res. 2007;462:122-9.
[14] Tateiwa T, Takahashi Y, Pezzotti G, Shishido T, Masaoka T, Sano K, et al. Does artificial aging correctly predict the long-term in-vivo degradation behavior in zirconia hip prostheses? Biomed Mater Eng. 2020;31:107-17.
[15] Allain J, Le Mouel S, Goutallier D, Voisin MC. Poor eight-year survival of cemented zirconia-polyethylene total hip replacements. J Bone Joint Surg Br. 1999;81:835-42.
[16] Hernigou P, Bahrami T. Zirconia and alumina ceramics in comparison with stainless-steel heads. Polyethylene wear after a minimum ten-year follow-up. J Bone Joint Surg Br. 2003;85:504-9.
[17] Norton MR, Yarlagadda R, Anderson GH. Catastrophic failure of the Elite Plus total hip replacement, with a Hylamer acetabulum and Zirconia ceramic femoral head. J Bone Joint Surg Br. 2002;84:631-5.
[18] Caton J, Bouraly JP, Reynaud P, Merabet Z. Phase Transformation in Zirconia Heads after THA Myth or Reality? Bioceramics in Joint Arthroplasty. 2004;26-27:73-4.
[19] Wroblewski M, Siney PD, Nagai H, Fleming PA. Wear of ultra-high-molecular-weight polyethylene cup articulating with 22.225 mm zirconia diameter head in cemented total hip arthroplasty. J Orthop Sci. 2004;9:253-5.
[20] Denry I, Kelly JR. Emerging ceramic-based materials for dentistry. J Dent Res. 2014;93:1235-42.
[21] Zhang Y, Lawn BR. Novel Zirconia Materials in Dentistry. J Dent Res. 2018;97:140-7.
[22] Ban S, Sato H, Suehiro Y, Nakanishi H, Nawa M. Biaxial flexure strength and low temperature degradation of Ce-TZP/Al2O3 nanocomposite and Y-TZP as dental restoratives. Journal of biomedical materials research Part B, Applied biomaterials. 2008;87:492-8.
[23] Kim HT, Han JS, Yang JH, Lee JB, Kim SH. The effect of low temperature aging on the mechanical property & phase stability of Y-TZP ceramics. The journal of advanced prosthodontics. 2009;1:113-7.
[24] Pereira GK, Venturini AB, Silvestri T, Dapieve KS, Montagner AF, Soares FZ, et al. Low-temperature degradation of Y-TZP ceramics: A systematic review and meta-analysis. Journal of the mechanical behavior of biomedical materials. 2015;55:151-63.
[25] ISO 13356-2015. Implants for Surgery – Ceramic Materials Based on Yttria-stabilized Tetragonal Zirconia (Y-TZP). IntOrganStand 2015.
[26] Muñoz EM, Longhini D, Antonio SG, Adabo GL. The effects of mechanical and hydrothermal aging on microstructure and biaxial flexural strength of an anterior and a posterior monolithic zirconia. Journal of dentistry. 2017;63:94-102.
[27] Koenig V, Wulfman C, Derbanne M, Dupont N, Le Goff S, Tang M-L, et al. Aging of monolithic zirconia dental prostheses: Protocol for a 5-year prospective clinical study using ex vivo analyses. Contemp Clin Trials Commun. 2016;4:25-32.
[28] Koenig V, Bekaert S, Dupont N, Vanheusden A, Le Goff S, Douillard T, et al. Intraoral low-temperature degradation of monolithic zirconia dental prostheses: Results of a prospective clinical study with ex vivo monitoring. Dental materials : official publication of the Academy of Dental Materials. 2021;37:1134-49.

[29] Koenig V, Wulfman C, Bekaert S, Dupont N, Le Goff S, Eldafrawy M, et al. Clinical behavior of second-generation zirconia monolithic posterior restorations: Two-year results of a prospective study with Ex vivo analyses including patients with clinical signs of bruxism. Journal of dentistry. 2019;91:103229.
[30] Wulfman C, Djaker N, Dupont N, Ruse D, Sadoun M, Lamy la Chapelle M. Raman Spectroscopy Evaluation of Subsurface Hydrothermal Degradation of Zirconia. J Am Ceram Soc. 2012;95:2347-51.
[31] Clarke DRA, F. Measurement of the cristallographically transformed zone produced by fracture in ceramics containing tetragonal zirconia. Journal of the American Ceramic Society. 1982;65:284-8.
[32] Mainjot AK, Douillard T, Gremillard L, Sadoun MJ, Chevalier J. 3D-characterization of the veneer-zirconia interface using FIB nano-tomography. Dental materials : official publication of the Academy of Dental Materials. 2013;29:157-65.
[33] Zhang F, Spies BC, Vleugels J, Reveron H, Wesemann C, Muller WD, et al. High-translucent yttria-stabilized zirconia ceramics are wear-resistant and antagonist-friendly. Dental materials : official publication of the Academy of Dental Materials. 2019;35:1776-90.
[34] Everall NJ. Confocal Raman microscopy: common errors and artefacts. Analyst. 2010;135:2512-22.
[35] Perrichon A, Reynard B, Gremillard L, Chevalier J, Farizon F, Geringer J. A testing protocol combining shocks, hydrothermal ageing and friction, applied to Zirconia Toughened Alumina (ZTA) hip implants. Journal of the mechanical behavior of biomedical materials. 2017;65:600-8.
[36] Maccauro G, Piconi C, Burger W, Pilloni L, De Santis E, Muratori F, et al. Fracture of a Y-TZP ceramic femoral head. Analysis of a fault. J Bone Joint Surg Br. 2004;86:1192-6.
[37] Lanone S, Rogerieux F, Geys J, Dupont A, Maillot-Marechal E, Boczkowski J, et al. Comparative toxicity of 24 manufactured nanoparticles in human alveolar epithelial and macrophage cell lines. Part Fibre Toxicol. 2009;6:14.
[38] Karunakaran G, Suriyaprabha R, Manivasakan P, Yuvakkumar R, Rajendran V, Kannan N. Screening of in vitro cytotoxicity, antioxidant potential and bioactivity of nano- and micro-ZrO2 and -TiO2 particles. Ecotoxicol Environ Saf. 2013;93:191-7.
[39] Dalal A, Pawar V, McAllister K, Weaver C, Hallab NJ. Orthopedic implant cobalt-alloy particles produce greater toxicity and inflammatory cytokines than titanium alloy and zirconium alloy-based particles in vitro, in human osteoblasts, fibroblasts, and macrophages. Journal of biomedical materials research Part A. 2012;100:2147-58.
[40] Demir E, Burgucu D, Turna F, Aksakal S, Kaya B. Determination of TiO2, ZrO2, and Al2O3 nanoparticles on genotoxic responses in human peripheral blood lymphocytes and cultured embyronic kidney cells. J Toxicol Environ Health A. 2013;76:990-1002.
[41] Soto K, Garza KM, Murr LE. Cytotoxic effects of aggregated nanomaterials. Acta biomaterialia. 2007;3:351-8.
[42] Otero-González L, García-Saucedo C, Field JA, Sierra-Álvarez R. Toxicity of TiO_2, ZrO_2, Fe^0, Fe_2O_3, and Mn_2O_3 nanoparticles to the yeast, Saccharomyces cerevisiae. Chemosphere. 2013;93:1201-6.
[43] Landsiedel R, Ma-Hock L, Hofmann T, Wiemann M, Strauss V, Treumann S, et al. Application of short-term inhalation studies to assess the inhalation toxicity of nanomaterials. Part Fibre Toxicol. 2014;11:16.
[44] Brunner TJ, Wick P, Manser P, Spohn P, Grass RN, Limbach LK, et al. In vitro cytotoxicity of oxide nanoparticles: comparison to asbestos, silica, and the effect of particle solubility. Environ Sci Technol. 2006;40:4374-81.
[45] Ye M, Shi B. Zirconia Nanoparticles-Induced Toxic Effects in Osteoblast-Like 3T3-E1 Cells. Nanoscale Res Lett. 2018;13:353.
[46] Tholey MJ, Berthold C, Swain MV, Thiel N. XRD2 micro-diffraction analysis of the interface between Y-TZP and veneering porcelain: role of application methods. Dental materials : official publication of the Academy of Dental Materials. 2010;26:545-52.
[47] Tholey MJ, Swain MV, Thiel N. SEM observations of porcelain Y-TZP interface. Dental materials : official publication of the Academy of Dental Materials. 2009;25:857-62.
[48] Bergamo E, da Silva WJ, Cesar PF, Del Bel Cury AA. Fracture Load and Phase Transformation of Monolithic Zirconia Crowns Submitted to Different Aging Protocols. Operative dentistry. 2016;41:E118-E30.
[49] Camposilvan E, Leone R, Gremillard L, Sorrentino R, Zarone F, Ferrari M, et al. Aging resistance, mechanical properties and translucency of different yttria-stabilized zirconia ceramics for monolithic dental crown applications. Dental materials : official publication of the Academy of Dental Materials. 2018;34:879-90.
[50] Naik VB, Jain AK, Rao RD, Naik BD. Comparative evaluation of clinical performance of ceramic and resin inlays, onlays, and overlays: A systematic review and meta analysis. J Conserv Dent. 2022;25:347-55.
[51] Pjetursson BE, Sailer I, Latyshev A, Rabel K, Kohal RJ, Karasan D. A systematic review and meta-analysis evaluating the survival, the failure, and the complication rates of veneered and monolithic all-ceramic implant-supported single crowns. Clin Oral Implants Res. 2021;32 Suppl 21:254-88.
[52] Hansen TL, Schriwer C, Oilo M, Gjengedal H. Monolithic zirconia crowns in the aesthetic zone in heavy grinders with severe tooth wear - An observational case-series. Journal of dentistry. 2018;72:14-20.

Figure captions

Figure 1: Study design

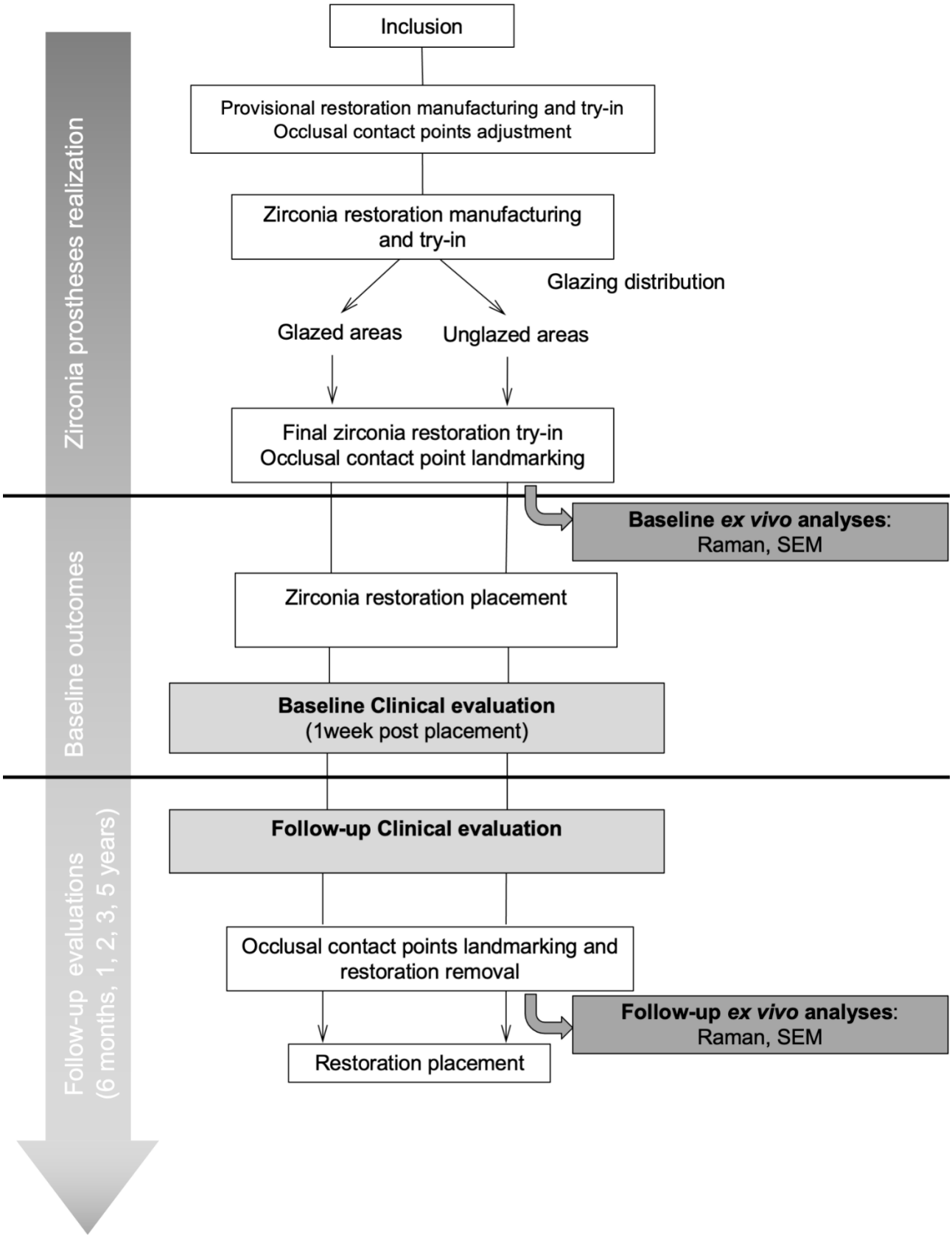

Figure 2: Realization of a Lava Plus zirconia crown on a natural tooth (a) Crown after intraoral try-in: the contact point areas with the opposite teeth were shaped in order to obtain a flat surface of a minimum of 1-2 mm^2. Registering of contact points on the masticatory surface, which is subjected to mechanical stress (MS+). Areas that will not be glazed are encircled with permanent ink. The lingual surface of the crown, which is not subjected to mechanical stress (MS-), is left unglazed (G-). b) For molars, two cusps have been randomly selected to remain unglazed (MS+G-). The two other cusps were glazed (MS+G+). (c) Glazed Lava Plus zirconia final crown. (d) Landmarking of areas to be analyzed after intraoral try-in. (e) Intraoral view of the MS+ surface after baseline evaluation and restoration placement. (f) MS- surface view.

Figure 3: Screw-retained Lava Plus zirconia crown on a dental implant. (a) Crown after intraoral try-in and registering of contact points with the opposite tooth (MS+). Areas that will not be glazed (G-) are encircled with permanent ink. The lingual surface of the crown (MS-) is left unglazed. For premolars, one cusp is randomly selected to remain unglazed. (b) Landmarking of the areas to be analyzed after intraoral try-in of the final zirconia crown. (c) Intraoral view of the MS+ surface after baseline evaluation and restoration placement. d) MS- surface view.

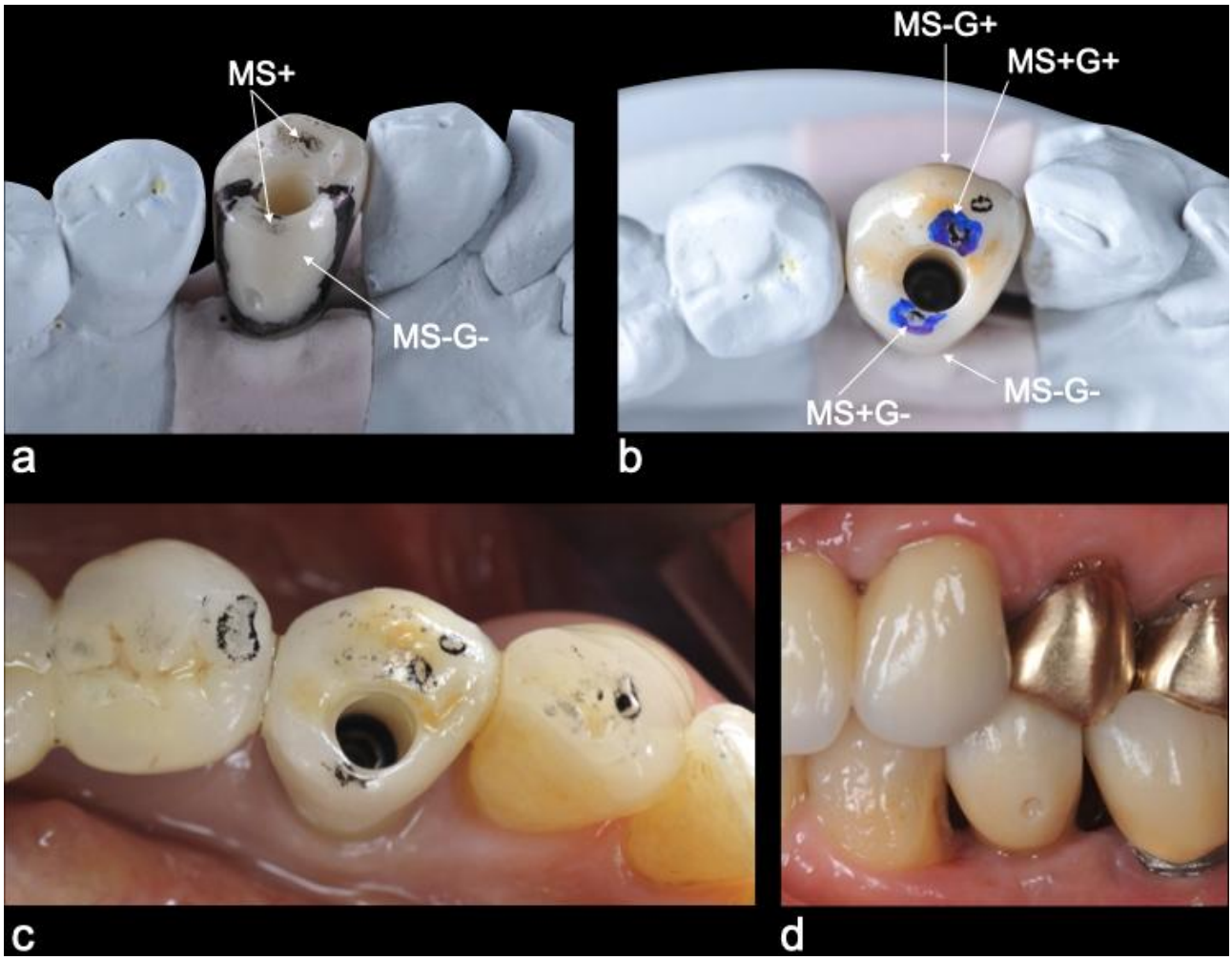

Figure 4: (a) Time evolution of the percentage of measurement points (MPs) with a $V_{fm} > 0,5\%$ (MPs+) globally and according to the type of area (MS+ or MS-). (b) Time evolution of the percentage of measurement points (MPs) with a $V_{fm} > 50\%$ (MPs+50%) globally and according to the type of area (MS+ or MS-). In each figure, the global evolution in MS- and MS+ areas is schematized by a straight line. Numbers indicate the total number of MPs at each evaluation time globally and according to the type of area (MS+ or MS-).

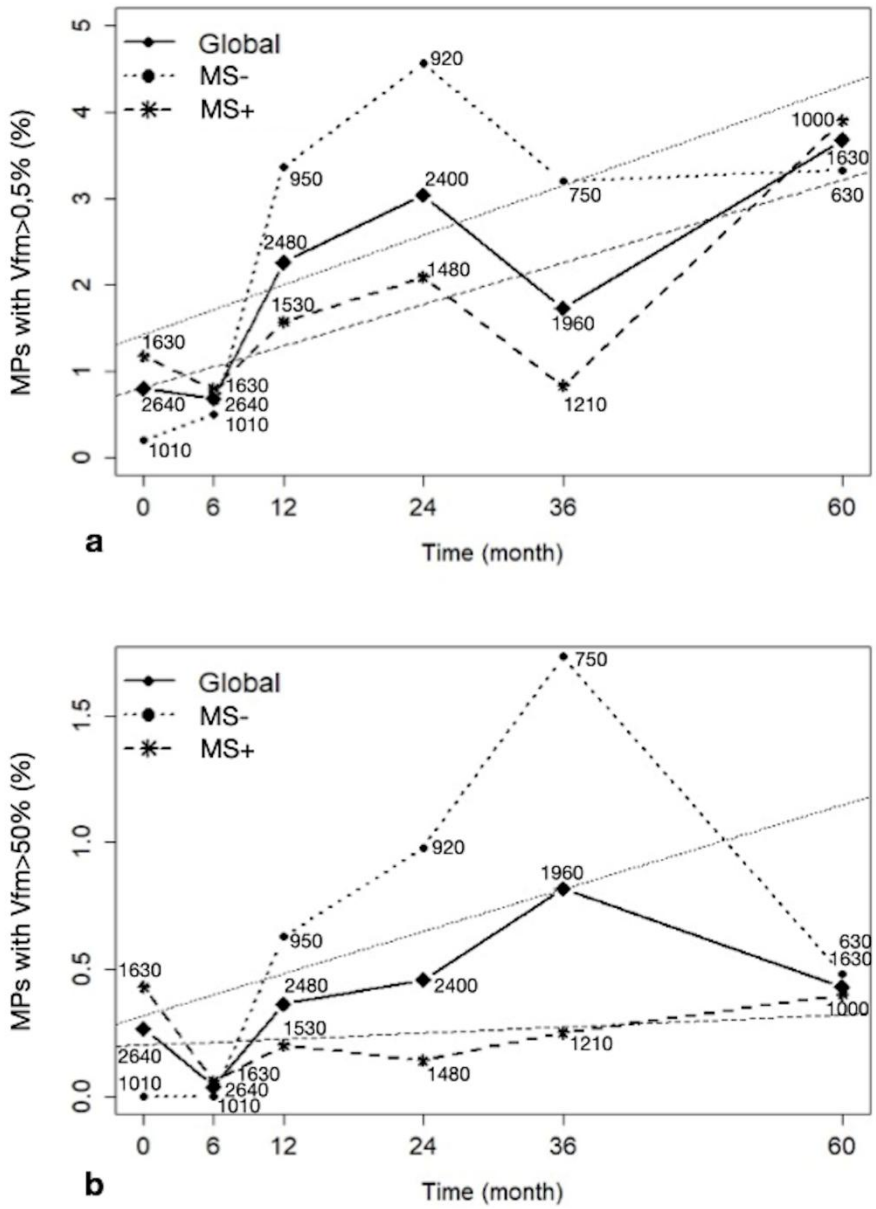

Figure 5: Scanning electron microscopy observation in tooth-supported dental crown. (a) MS+ areas (subjected to mechanical stress) at baseline. Light grey zones correspond to unglazed areas. (b) MS+ areas at 2-year follow-up: glaze is shown to wear out on contact points with the opposite tooth (white arrows). (c) MS+ areas at 5-year follow-up. (d) MS- area (not subjected to mechanical stress) at 2-year follow-up: glaze was shown to be intact.

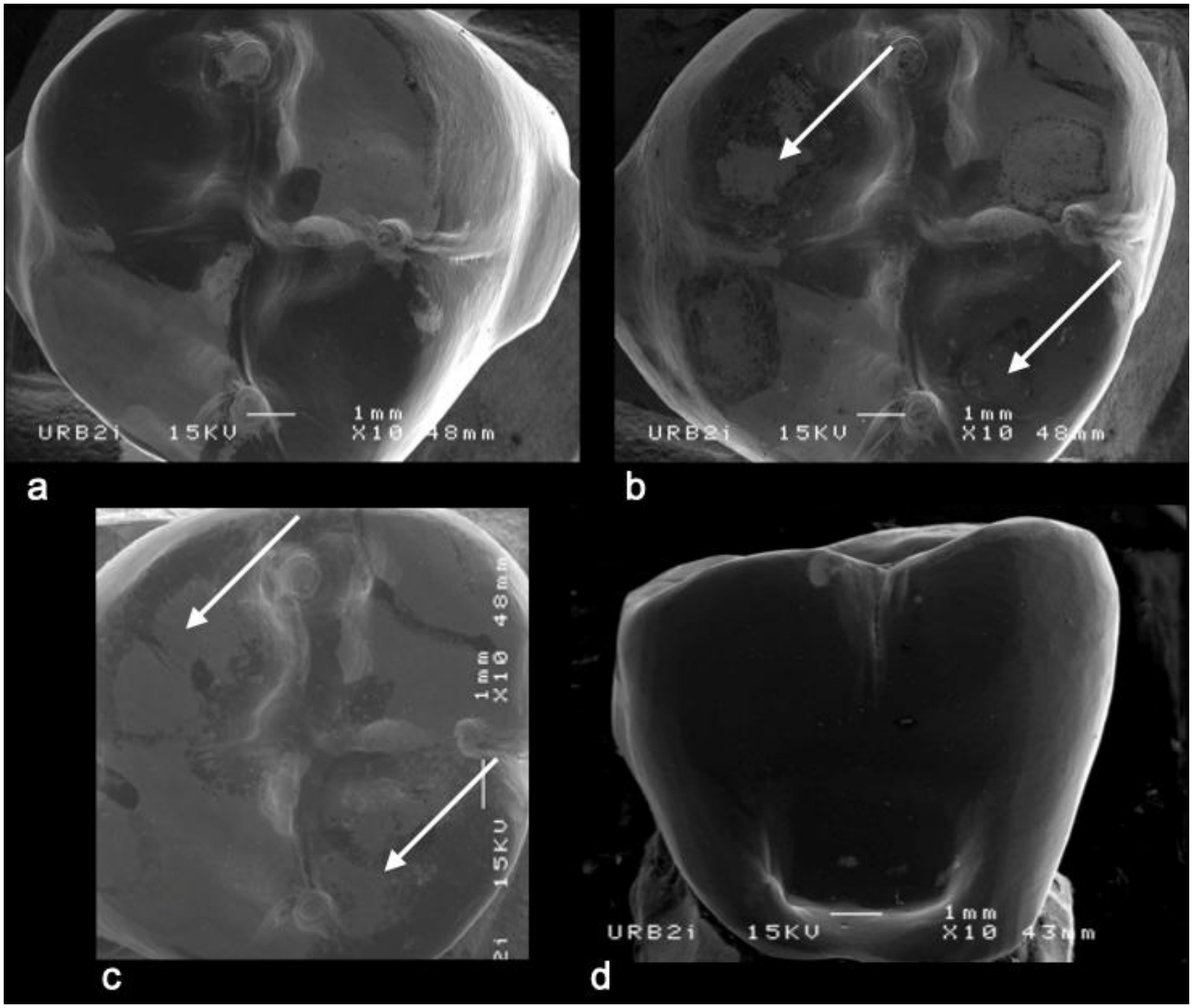

Figure 6: Raman mapping on dental crowns. Large-scale image (100×100 μm^2) with a scale from black (V_{fm}=0%) to bright orange (V_{fm}=maximum): (a) MS+ area (subjected to mechanical stress) and (b) MS- area (not subjected to mechanical stress) just machined (control); (d) MS+ area and (h) MS- area at 3 years. (l) MS+ area and (p) MS- area at 5 years. Related spectra are presented in figures c, e, h, k and n, respectively. The yellow spectrum shows peaks around 180 cm^{-1}, which are characteristic of the monoclinic phase (encircled in red). No *t-m* transformation was detected at baseline. High-resolution mapping (25×25 μm^2) was carried out on the detected transformed grains (encircled in red) with a scale from violet (V_{fm}=0%) to red (V_{fm}=maximum) on the MS+ (f) (l) and MS- (i) (o) areas.

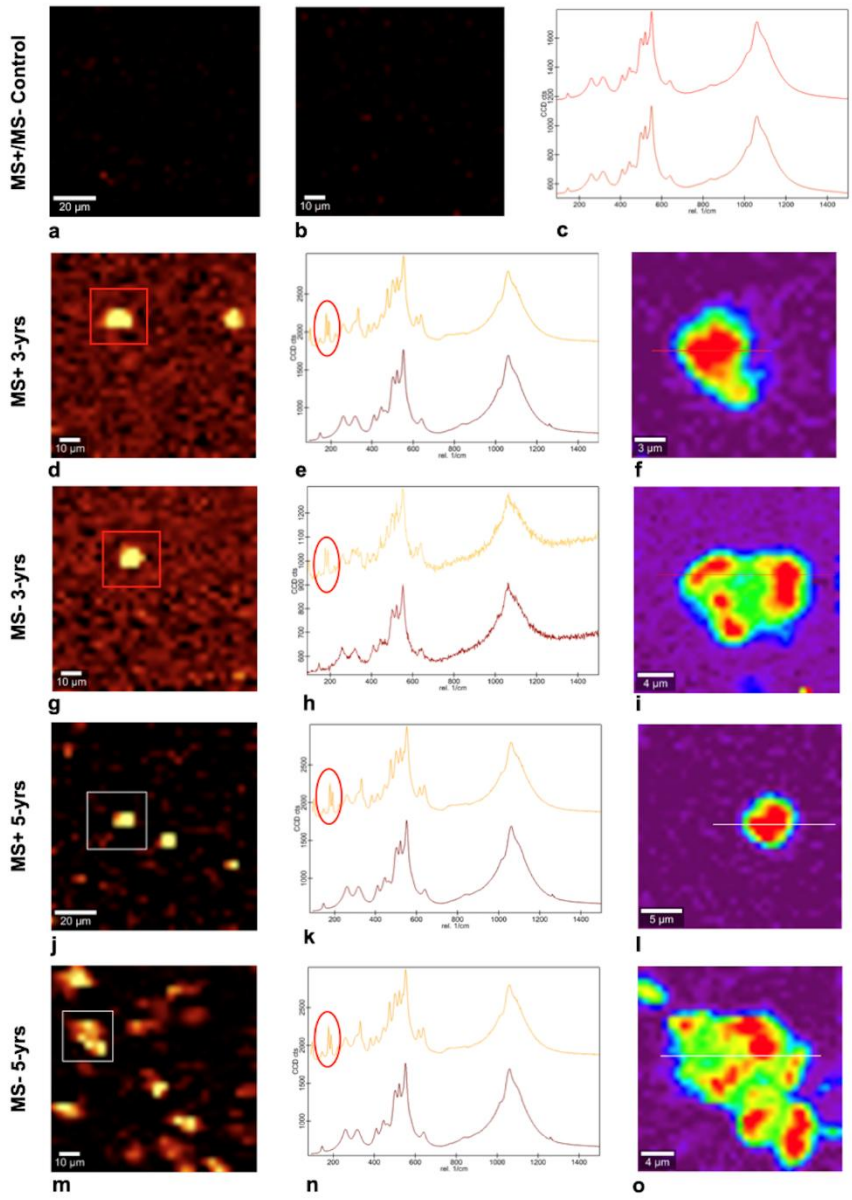

Figure 7: (a) High-resolution SEM observation of a typical dental crown just machined (control), MS- area (not subjected to mechanical stress), (b) of the same crown, MS+ area (subjected to mechanical stress), (c) High-resolution SEM observation of a dental crown at 2-year follow-up, MS- area, (d) of the same crown, MS+ area, (e) at 5-year follow-up, MS- area, (f) at 5-year follow-up, MS+ area. The surface of the material of the control crown is not porous and the grains are intact. After 2 years, on the MS- areas, the grain aspect is typical of the classical LTD process. However, on MS+ areas, SEM images illustrate the effect of the tribological stress on contact point areas with grain pull-out, low-density material, and crushing of remaining grains, which appear plastically deformed. After 5 years, similar scanning electron microscopy images were observed in MS- areas than in MS+ areas.

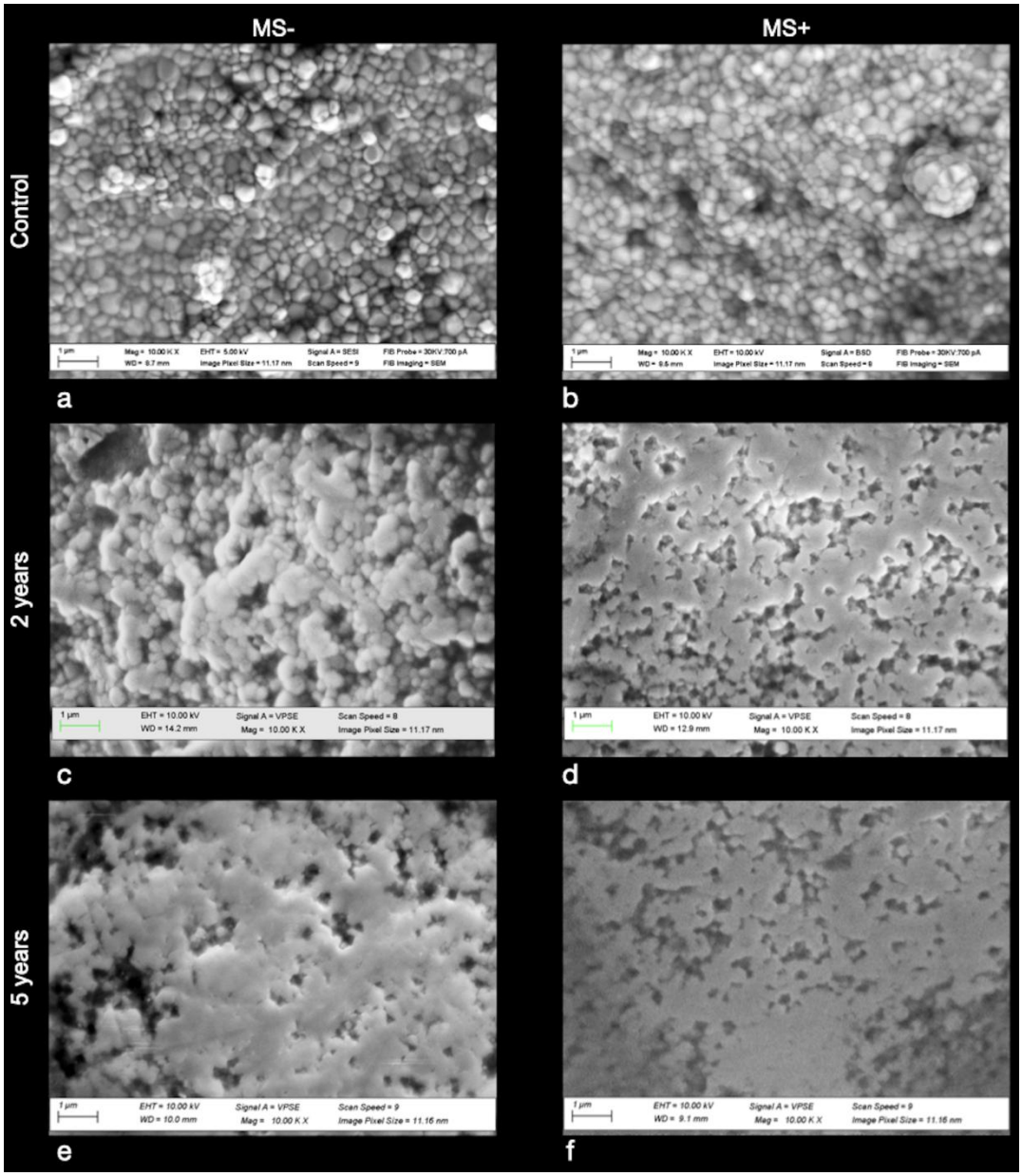

Figure 8: Scanning electron microscopy images of focused ion beam cross-sections.

(a) and (b): MS+ surface (subjected to mechanical stress) of the control dental crown shown in Figure 3. Monoclinic grains are not observed.

(c) MS+ surface of the dental crown at the 5-year follow-up shown in Figure 3: differences in the microstructure and a sharp boundary between the heterogeneous transformed regions with its martensitic structure and the homogeneous unaffected region are clearly visible (delimited by a red line), (d) same image at 30.00 KX magnification: no transformed grains were observed beyond 1 µm, (e) same image at 30.00 KX magnification: some cracks were observed on the surface (white arrows).

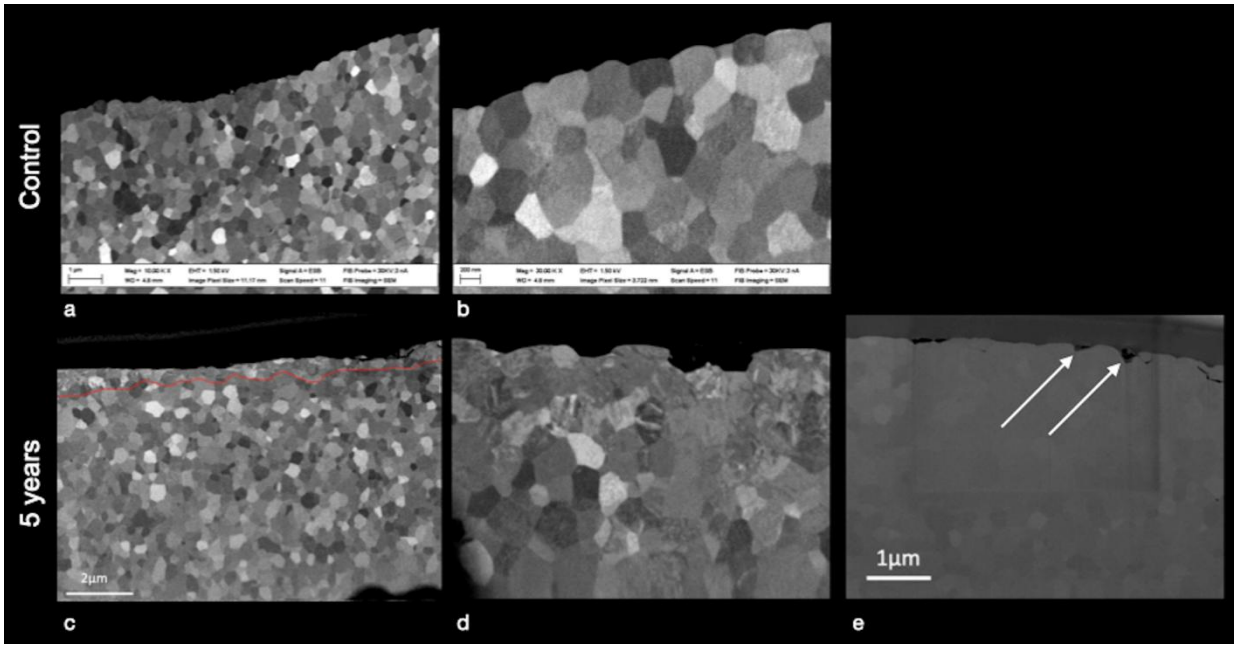

Figure 9: Schematic illustration of the low-temperature degradation process in the presence of mechanical stress, which is characterized by a grain pull-out from clusters of transformed grains.

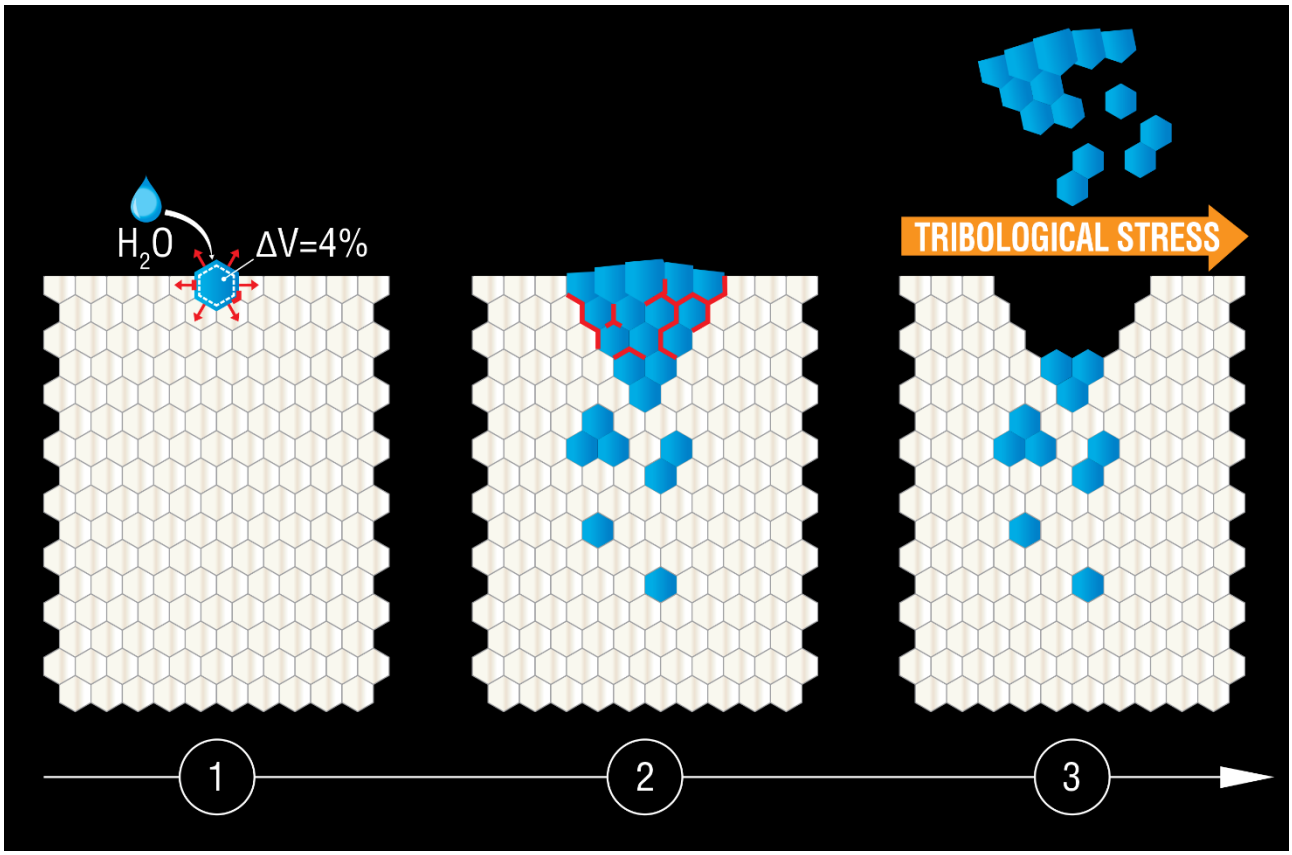

Table 1: Sample description in terms of patients, tooth-elements, *ex vivo* analysed areas, and Raman measurement points (MPs). MS+: areas subjected to mechanical stress, MS-: areas not subjected to mechanical stress, G+: glazed areas, G-: unglazed areas.

Patients (n tot = 47)	**% (n)**
Sex	
Female	70.2 (33)
Male	29.8 (14)
Crowns (n tot= 101)	**% (n)**
Support	
Tooth	12.9 (13)
Implant	87.1 (88)
Tooth type	
Premolar	38.6 (39)
Molar	61.4 (62)
Analyzed areas (n tot= 528)	**% (n)**
MS+ (n = 326)	
MS+G+	55.5 (181)
MS+G-	44.5 (145)
MS- (n = 202)	
MS-G+	50 (101)
MS-G-	50 (101)
Raman measurement points (MPs) (n tot= 2640)	**% (n)**
MS+ (n = 1630)	
MS+G+	55.5 (905)
MS+G-	44.5 (725)
MS- (n = 1010)	
MS-G+	50 (505)
MS-G-	50 (505)

Table 2: Areas with at least one transformation-positive measurement point (MP+). Distribution of the number of MPs+ per transformation-positive area at each evaluation time and for areas subjected to mechanical stress (MS+) and not subjected to mechanical stress (MS-). Different superscripts (within the column) denote that there were significant differences between the evaluation times. *P*-values are from a generalized linear mixed model with a level of significance of $p<0.05$.

	n transformation-positive areas/ n tot areas (%)	Transformation-positive areas, which on 5 MPs, show:			
		4 zero values n (%)	3 zero values n (%)	2 zero values n (%)	1 zero values n (%)
Global					
Baseline	21/528 (3.98)[a]	21 (100)	0 (0)	0 (0)	0 (0)
6 months	18/528 (3.41)[a]	18 (100)	0 (0)	0 (0)	0 (0)
1 year	49/496 (9.88)[b,c]	42 (85.71)	7 (14.29)	0 (0)	0 (0)
2 years	57/480 (11.88)[b]	46 (80,70)	7 (12.28)	3 (5.26)	1 (1.75)
3 years	27/392 (6.89)[c]	20 (74.1)	7 (25.9)	0	0
5 years	44/326 (13.50)[b]	31 (70.4)	11 (25.0)	1 (2.3)	1 (2.3)
MS-					
Baseline	2/202 (0.99)[d]	2 (100)	0 (0)	0 (0)	0 (0)
6 months	5/202 (2.48)[d]	5 (100)	0 (0)	0 (0)	0 (0)
1 year	26/190 (13.68)[e,f]	20 (76.92)	6 (23.08)	0 (0)	0 (0)
2 years	32/184 (17.39)[e,g]	25 (78.13)	5 (15.63)	1 (3.13)	1 (3.13)
3 years	18/150 (12.0)[e]	12 (66.7)	6 (33.3)	0	0
5 years	18/126 (14.29)[f,g]	15 (83.3)	3 (16.7)	0	0
MS+					
Baseline	19/326 (5.83)[h,i]	19 (100)	0 (0)	0 (0)	0 (0)
6 months	13/326 (3.99)[h]	13 (100)	0 (0)	0 (0)	0 (0)
1 year	23/306 (7.52)[h,j]	22 (95.65)	1 (4.35)	0 (0)	0 (0)
2 years	25/296 (8.45)[i,j,k]	21 (84.0)	2 (8.0)	2 (8.0)	0 (0)
3 years	9/242 (3.72)[h,l]	8 (88.9)	1 (11.1)	0	0
5 years	26/200 (13.0)[k,l]	16 (61.5)	8 (30.8)	1 (3.9)	1 (3.9)

Table 3: Results of Raman analyses: number of measurement points (MPs), transformation-positive MPs with $V_{fm} > 0\%$ (MPs+), transformation-positive MPs with $V_{fm} > 50\%$ (MPs+50%) and mean V_{fm} value with median, interquartile range (IQR) and range (min–max) at each evaluation time and for areas subjected to mechanical stress (MS+) and not subjected to mechanical stress (MS-). Different superscripts (within the column, for each variable) denote that there were significant differences between the evaluation times. For the time evolution of the transformation, *p*-values are from a generalized linear mixed model with the level of significance of $p<0.05$ and were not applicable (NA) for the axial MPs +50% at baseline and 6 months.

For the transformation percentage over time, *p*-values were obtained from a zero-inflated non-negative binomial regression for repeated measurements, with a significance level of $p<0.05$.

		MPs (n tot)	MPs+ n (%)	MPs+50% n (%)	Mean V_{fm} (%)	Median	IQR	Min	Max
Global	Baseline	2640	21 (0.80)[a]	7 (0.27)[a]	0.26[a]	0.00	0.00	0.00	90.00
	6 months	2640	18 (0.68)[a]	1 (0.04)[b]	0.12[b,c]	0.00	0.00	0.00	93.00
	1 year	2480	56 (2.26)[b,c]	9 (0.36)[a]	0.52[d,e]	0.00	0.00	0.00	96.00
	2 years	2400	73 (3.04)[b]	11 (0.46)[a,c]	0.62[b,d]	0.00	0.00	0.00	90.00
	3 years	1960	34 (1.73)[c]	16 (0.82)[c,d]	0.78[a,c,e]	0.00	0.00	0.00	90.00
	5 years	1630	60 (3.68)[b]	7 (0.43)[a,d]	0.63[b]	0.00	0.00	0.00	90.00
MS-	Baseline	1010	2 (0.20)[a]	0 (0.0)[NA]	0.02[a,b]	0.00	0.00	0.00	12.00
	6 months	1010	5 (0.50)[a]	0 (0.0)[NA]	0.06[a]	0.00	0.00	0.00	21.00
	1 year	950	32 (3.37)[b,c]	6 (0.63)[a]	0.87[a,c]	0.00	0.00	0.00	96.00
	2 years	920	42 (4.57)[b,d]	8 (0.87)[a]	1.22[a]	0.00	0.00	0.00	90.00
	3 years	750	24 (3.20)[b]	13 (1.73)[a]	1.61[b,c]	0.00	0.00	0.00	90.00
	5 years	630	21 (3.33)[c,d]	3 (0.48)[a]	0.73[a]	0.00	0.00	0.00	90.00
MS+	Baseline	1630	19 (1.17)[a,b]	7 (0.43)[a]	0.41[a]	0.00	0.00	0.00	90.00
	6 months	1630	13 (0.80)[a]	1 (0.06)[b]	0.15[b,c]	0.00	0.00	0.00	93.00
	1 year	1530	24 (1.57)[a,c]	3 (0.20)[b]	0.31[b,d]	0.00	0.00	0.00	93.00
	2 years	1480	31 (2.09)[b,c,d]	3 (0.20)[b]	0.25[b]	0.00	0.00	0.00	64.00
	3 years	1210	10 (0.83)[a,e]	3 (0.25)[b]	0.26[a,c,d,e]	0.00	0.00	0.00	90.00
	5 years	1000	39 (3.90)[d,e]	4 (0.40)[b]	0.57[b,e]	0.00	0.00	0.00	90.00